Accepted by The Astrophysical Journal
Preprint typeset using LaTeX style emulateapj v. 11/10/09

arXiv:0911.0041v2 [astro-ph.CO] 29 Jun 2010

MODELING THE LARGE SCALE BIAS OF NEUTRAL HYDROGEN

Felipe A. Marín[1,2], Nickolay Y. Gnedin[3,1,2], Hee-Jong Seo[3] and Alberto Vallinotto[3]

Draft version July 1, 2010

ABSTRACT

We present new analytical estimates of the large scale bias of neutral hydrogen (H I) We use a simple, non-parametric model which monotonically relates the total mass of a halo $M_{\rm tot}$ with its H I mass $M_{\rm H\,I}$ at zero redshift; for earlier times we assume limiting models for the $\Omega_{\rm H\,I}$ evolution consistent with the data presently available, as well as two main scenarios for the evolution of our $M_{\rm H\,I}$ - $M_{\rm tot}$ relation. We find that both the linear and the first nonlinear bias terms exhibit a strong evolution with redshift, regardless of the specific limiting model assumed for the H I density over time. These analytical predictions are then shown to be consistent with measurements performed on the Millennium Simulation. Additionally, we show that this strong bias evolution does not sensibly affect the measurement of the H I power spectrum.

Subject headings: cosmology: large-scale structure of universe, diffuse radiation

1. INTRODUCTION

The 21cm emission line of neutral hydrogen has been the workhorse of astronomy for over 50 years. Its use for galactic astronomy cannot be overestimated, and it now promises to revolutionize cosmology as well (cf. Furlanetto et al. 2006; Barkana & Loeb 2007; Pritchard & Loeb 2008; Mao et al. 2008; Visbal et al. 2008, and references therein).

Compared to present probes of large-scale structure, the 21 cm intensity mapping technique (Chang et al. 2008a; Wyithe et al. 2008a) offers three advantages. First, it allows to reconstruct the spatial distribution of H I in the universe over volumes much larger than the ones currently probed by galaxy redshift surveys. Since the precision with which the power spectrum of density fluctuations can be measured is approximately proportional to the number of independent Fourier modes that fit into the survey volume, a larger survey volume leads to higher precision in the measured power spectrum and hence cosmological parameters (Loeb & Wyithe 2008). Second, 21 cm intensity mapping allows to probe a very wide range of redshifts and to map H I distribution in space and time not only for the epoch after reionization ($z \lesssim 6$) but also during reionization and even in the so-called dark ages, before the first galaxies were formed ($z \gtrsim 20$). Third, using radio telescopes is one of the most economical ways to probe the dark energy evolution among all current and planned experiments, although several crucial advances in calibration and foreground removal must be made for the intensity mapping approach to reach its stated goals.

As a dark energy probe, 21 cm intensity mapping is primarily useful for measuring the baryon acoustic oscillations (BAO) in the matter power spectrum (Wyithe et al. 2008b; Chang et al. 2008b; Wyithe et al. 2008a; Ansari et al. 2008; Seo et al. 2010), which provides important information on constraining cosmological models and parameters. Measurements of the scale of the BAO in the matter power spectrum as a function of redshift, when combined with the true physical scale, i.e., the sound horizon scale measured from the cosmic microwave background (CMB), probe the angular diameter distances and Hubble parameters to various redshifts, and therefore dark energy properties (see, for instance, Hu & White 1996; Eisenstein et al. 1998; Eisenstein 2002; Blake & Glazebrook 2003; Linder 2003; Hu & Haiman 2003; Seo & Eisenstein 2003). The distinct oscillatory feature of the BAO allows us to isolate and measure the BAO information independent of the overall broadband shape of the HI power spectrum. Therefore in principle BAO measurements do not require a knowledge of the HI bias, i.e., the relation between the neutral hydrogen and the total matter clustering, which affects the overall shape of the HI power spectrum.

However, understanding the HI bias is important for the 21cm BAO surveys in the following ways. First the prediction of the signal to noise of the BAO measurements is sensitive to the knowledge of the clustering bias of HI (Chang et al. 2008b; Seo et al. 2010). Second, understanding HI bias will help us to extract cosmological information from the broadband shape of the power spectrum in addition to the BAO. Third, the nonlinear effects on the BAO, such as the degradation and the shift of the feature, may differ for different biased tracers (e.g., Padmanabhan & White 2009; Metha et al. 2010). Knowing the properties of HI bias will allow us to approximately estimate the degree of the expected nonlinear effect on the BAO in the HI distribution.

In this work, we focus on two critical aspects of the large-scale H I bias: its dependence on the relation between H I mass and halo mass and its evolution with redshift. To study the first aspect, we use a non-parametric model where we assume a one-to-one correspondence between a H I mass present in a dark matter halo $M_{\rm H\,I}$ and the total mass $M_{\rm tot}$ of this halo. Using this $M_{\rm H\,I} - M_{\rm tot}$ relation we estimate the large-scale bias of the H I using a model containing elements on the halo occupation

[1] Department of Astronomy & Astrophysics, The University of Chicago, Chicago, IL 60637 USA; fmarinp@oddjob.uchicago.edu
[2] Kavli Institute for Cosmological Physics and Enrico Fermi Institute, The University of Chicago, Chicago, IL 60637 USA
[3] Center for Particle Astrophysics, Fermi National Accelerator Laboratory, P.O. Box 500 Kirk Rd. & Pine St., Batavia, IL 60510-0500; gnedin@fnal.gov, sheejong@fnal.gov, avalli@fnal.gov

distribution (HOD) formalism and the H I mass function measured at $z = 0$ (Zwaan et al. 2005). We then use this relation to paint H I on Millennium Simulation halos (Springel et al. 2005) and to measure the power spectrum of neutral hydrogen in order to test our model assumptions.

With respect to the redshift evolution of the bias, it is absolutely critical to know how the H I mass function evolves with time. However, to the best of our knowledge, little is known about the redshift evolution of H I both on the theoretical and the observational sides (but see Wyithe et al. 2009). A detailed study of the bias evolution requires two extra pieces of information which are currently poorly constrained by observational data: the evolution of the total HI mass in the universe and the evolution of the HI mass function. For both of these, we empirically assume limiting evolution models consistent with the few available data that should bracket the actual evolution. We then proceed to predict the bias evolution in these scenarios, being aware of the fact that the actual evolution will lie somewhere in between these limiting cases.

The paper is organized as follows. In §2 we introduce the basics of our model, we derive the relation $M_{\rm HI} - Mtot$ at $z = 0$, we introduce the limiting cases for its evolution and we define the bias. In §3 we present our main results: analytic predictions for the evolution of HI bias, measurement of its scale dependence on the Millennium Simulation and how it would affects measurements of the power spectrum. Finally, we conclude in §4. To compare analytical and numerical results, throughout the paper we use a flat ΛCDM cosmology with $\Omega_M = 0.25$, $\sigma_8 = 0.9$, Hubble parameter $h = 0.73$ and initial power spectrum index of $n_s = 1$, consistent with the cosmological parameters used in the Millennium Simulation.

2. BACKGROUND

2.1. *Basic formalism*

The HOD model (cf. Cooray & Sheth 2002; Berlind & Weinberg 2002, and references therein) provides a parameterized prescription for the spatial distribution of objects that can be found inside dark matter halos. Originally inspired to model the distribution of galaxies, it can also be used to model the spatial distributions of other astronomical objects, such as the neutral hydrogen clouds. The advantage in using this approach is that the problem of deriving the spatial distribution naturally falls into two separate parts: the first part is concerned with the distribution of halos in the universe, and the second part involves how objects (i.e., galaxies, hydrogen clouds, etc) populate these halos. In this work we use some of the elements of this HOD formalism to attempt to estimate the large-scale bias, i.e. in a quasi-linear regime, where the estimations of the 21 cm correlations for studying the BAO will take place.

The first component is a model for the distribution of dark halos in the universe. In the analytic approach, one specifies the halo mass function, $n(M)$, the spatial correlations of the halos, and the density profiles for halos of mass M, all based on halo collapse models and fits to N-body simulations.

To describe the mass function of dark matter halos (the spatial density of halos as a function of mass), we use the Sheth & Tormen mass function (Sheth et al. 2001; Sheth & Tormen 2002):

$$n_h(M) = \frac{\bar{\rho}_m}{M^2} \left| \frac{d \ln \sigma}{d \ln M} \right| f(\nu), \tag{1}$$

where $\bar{\rho}_m \equiv \Omega_m \rho_c$ is the average matter density in the universe at the epoch of observation, $\nu(M)$, defined by $\nu(M) \equiv \delta_c/\sigma(M, z)$, is the ratio between the threshold for growth of linear fluctuations $\delta_c = 1.69$ and the rms variance of a sphere of radius R (corresponding to a mass M) at redshift z

$$\sigma^2(R, z) = \int \frac{d^3k}{(2\pi)^3} \left|W(k, R)\right|^2 P(k, z). \tag{2}$$

Here, $P(k, z)$ is the linear matter power spectrum and $W(k, R)$ is the Fourier transform of a top-hat window of radius R. The function $f(\nu)$ motivated by the ellipsoidal collapse model (Sheth & Tormen 2002) is

$$f(\nu) = A\sqrt{\frac{2a\nu^2}{\pi}} \left[1 + (a\nu^2)^{-p}\right] e^{-a\nu^2/2}, \tag{3}$$

where for normalization purposes, $A = 0.322$, $p = 0.3$ and $a = 0.707$.

The second component is a model specifying how the objects under consideration (in the present case, the amount of neutral hydrogen) occupy the dark halos as a function of halo mass. In a HOD model, for the largest scales, we would be interested in the average number of galaxies $\langle N(M_{\rm tot})\rangle$ that populate a particular halo of mass $M_{\rm tot}$. In our case, we are interested in the average number of H I atoms, or equivalently the average mass of H I inside a halo. For the scope of this paper, which deals with large scale-bias, we are not using the complete HOD prescription: this would mean specifying the complete probability distribution function of $P(M_{\rm H\,I}|M_{\rm tot})$, where its higher moments contribute to the estimation of the bias on small, nonlinear scales; for large scale bias, we only need the average H I mass $\langle M_{\rm H\,I}(M_{\rm tot})\rangle$. When interested in the small-scale bias, details the spatial and velocity distribution of the H I inside the halos are needed; these are out of the scope of this paper (see for instance Bagla & Khandai 2009, Obreschkow et al. 2009 Wyithe et al. 2009 for treatments that include small-scale clustering).

In the following subsection, we explore different models for the neutral hydrogen mass function and the relations between the neutral hydrogen $M_{\rm H\,I}$ and the total mass of a halo $M_{\rm tot}$.

2.2. *Neutral Hydrogen Mass Function*

The neutral hydrogen mass function of galaxies in the local universe has been measured by the HIPASS survey (Zwaan et al. 2005). However, the masses of the halos that host galaxies with a given H I mass are not, generally, known. Thus, we need to construct a plausible model for the relation between the total mass of a halo $M_{\rm tot}$ and its neutral hydrogen mass $M_{\rm H\,I}$.

While such a relation does not have to be a simple function, models that assume a one-to-one correspondence between the galaxy luminosity and the

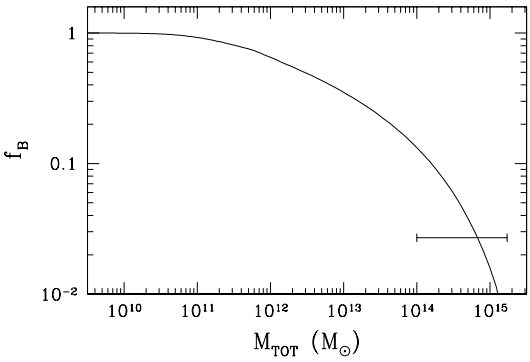

FIG. 1.— Fraction of blue galaxies as a function of total halo mass from matching the cumulative halo mass function and the observed SDSS galaxy luminosity function. The horizontal range shows the observed fraction on blue BCGs in the maxBCG galaxy cluster catalog (E. Rykoff, private communication).

halo mass (Colín et al. 1999; Kravtsov & Klypin 1999; Kravtsov et al. 2004) provide remarkably good fit not only to the galaxy correlation functions (Conroy et al. 2006; Marín et al. 2008) but also to a wide variety of observational tests (Nagai & Kravtsov 2005; Gnedin 2008; Volonteri & Gnedin 2009; Guo et al. 2009; Conroy & Wechsler 2009; Tinker & Conroy 2009). Therefore, it is tempting to assume such a relation between the H I mass and total halo mass as well, that is, to assign one HIPASS source to one dark matter halo.

There is one complication with such an approach – not all galaxies contain H I. Thus, we need to account for the fraction of galaxies that do. Unfortunately, there are no reliable observational measurements of the fraction of H I-rich galaxies as a function of galaxy mass or luminosity. Instead, we adopt a simple ansatz that all blue galaxies contain H I and all red galaxies do not. Then, we can use the abundance matching technique if we match the abundances of HIPASS and blue galaxies.

Specifically, the relation between the total mass of a dark matter halo $M_{\rm tot}$ and its H I mass $M_{\rm H\,I}$ can be obtained by matching the two cumulative mass functions,

$$n_{\rm H\,I}(> M_{\rm H\,I}) = n_B(> M_{\rm tot}), \qquad (4)$$

where $n_{\rm H\,I}$ is the observed cumulative mass function (Zwaan et al. 2005) and

$$n_B(> M_{\rm tot}) = \int_{M_{\rm tot}}^{\infty} dM f_B(M) n_h(M). \qquad (5)$$

In the last equation, f_B is the fraction of blue galaxies as a function of halo mass.

That fraction can be computed from the measured Sloan Digital Sky Survey (SDSS) red and blue galaxy luminosity functions (Montero-Dorta & Prada 2009) using the same abundance-matching technique. Namely, using the total SDSS luminosity function from Montero-Dorta & Prada (2009) we first match halo masses to r-band magnitudes as

$$n_{\rm gal}(< m_r) = \int_{M_{\rm tot}}^{\infty} dM n_h(M); \qquad (6)$$

such a matching gives us a relation between a galaxy magnitude m_r and the halo mass $M_{\rm tot}$. Then, for each m_r (and, hence, $M_{\rm tot}$) we compute the fraction of blue

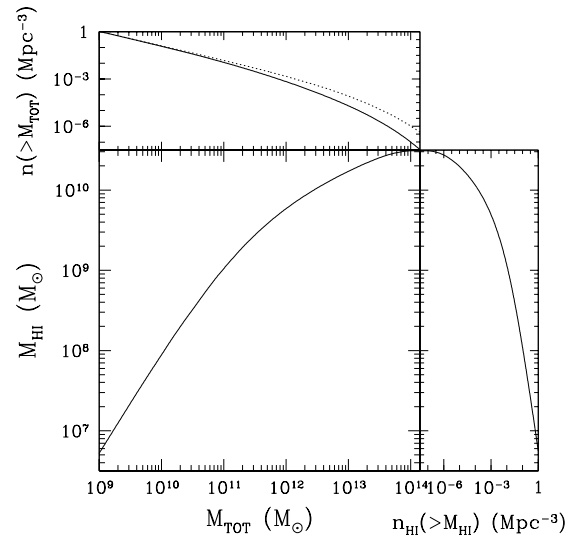

FIG. 2.— Cumulative mass function of dark matter halos of blue galaxies (top panel), the cumulative H I mass function of galaxies (from Zwaan et al. 2005, right panel), and the relation between the galaxy H I mass and its halo mass (central panel) obtained by matching the two, at $z = 0$. The dotted line in the top panel shows the cumulative mass function of all dark matter halos, hosting both blue and red galaxies.

galaxies from the measured blue galaxy luminosity function (Montero-Dorta & Prada 2009). The so-measured blue galaxy fraction is shown in Figure 1 together with am estimate of the blue BCG fraction from the maxBCG galaxy cluster catalog (E. Rykoff, private communication). Estimates of the blue BCG fraction in X-ray selected clusters usually give substantially larger numbers (Bildfell et al. 2008); however, because X-ray emission is likely to correlate with the existence of a cooling flow (and, hence, a blue BCG), the latter estimates should be taken as upper limits (E. Rykoff, private communication).

The resulting matching between the H I mass of a galaxy and its total mass from Equation (4) is shown in Figure 2. The relation between $M_{\rm H\,I}$ and $M_{\rm tot}$ from the central panel allows us to compute the clustering properties of H I from the known clustering properties of the dark matter halos.

Unfortunately, little is known about the H I mass function beyond $z \approx 0.1$. To obtain the $M_{\rm H\,I}$ - $M_{\rm tot}$ matching at higher redshifts, we therefore must extrapolate the observed H I mass function to earlier times. This extrapolation is, of course, not unique and it requires two ingredients: the evolution of the total H I mass and how the H I mass is distributed among halos. To make the matter even worse, the observational constraints on the total H I mass density in the universe $\rho_{\rm H\,I}$ (or, equivalently, the cosmological density parameter $\Omega_{\rm H\,I}$) are imprecise. Figure 3 shows a representative sample of these constraints for a range of redshifts (Zwaan et al. 2005; Prochaska et al. 2005; Rao et al. 2006). While at $z \approx 0$ and $z \gtrsim 2$ the measurements are reasonably robust, at intermediate redshifts the error bars are large and the behavior is non-monotonic. Therefore, to explore a wide enough range of possible evolutionary histories of $\Omega_{\rm H\,I}$, we choose three representative models.

- Model A provides a reasonable fit to all data

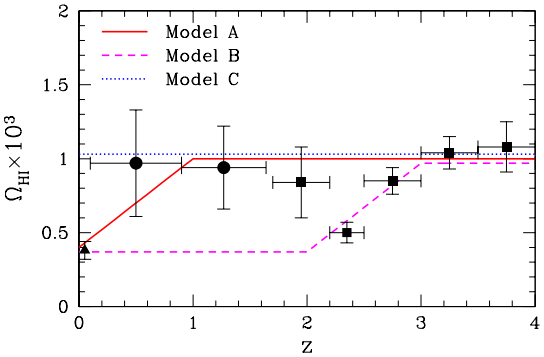

FIG. 3.— Three models (A, B, and C) for the redshift evolution of the total H I density that we explore in this paper. The lines for the models are slightly shifted vertically for clarity – all models adopt $\Omega_{\rm H\,I} = 10^{-3}$ at $z > 3$. Black symbols with error bars show the observational measurements from Zwaan et al. (2005) (triangle), Rao et al. (2006) (circles), and Prochaska et al. (2005) (squares).

points except for a single $z \approx 2.3$ point from Prochaska et al. (2005).

- Model B follows the suggestion of Prochaska & Wolfe (2009), who argue that $\Omega_{\rm H\,I}$ does not evolve between $z = 0$ and $z \approx 2$. Since it provides a plausible lower limit to the redshift evolution of $\Omega_{\rm H\,I}$, we use this model even if it ignores the measurements of Rao et al. (2006).

- In the same spirit, Model C serves as an upper limit to the possible $\Omega_{\rm H\,I}(z)$. Formally, it is inconsistent with the HIPASS measurement, but we assume that $\Omega_{\rm H\,I}$ in Model C increases rapidly from the HIPASS value of 3.8×10^{-4} to about 10^{-3} within a redshift interval $\Delta z \ll 1$.

To fully specify the H I mass function we then need to address how the total H I mass is distributed among halos as a function of redshift. If the shape of the H I mass function is approximately preserved at $z > 0$, then

$$n_{\rm H\,I}(> M_{\rm H\,I}, z) = q_N(z) n_0(> q_M(z) M_{\rm H\,I}), \qquad (7)$$

where $n_0(> M_{\rm H\,I})$ is the observed cumulative HIPASS mass function (Zwaan et al. 2005) at $z = 0$. The two quantities q_N and q_M are not independent; for a given evolutionary history of neutral hydrogen contents of the universe $\rho_{\rm H\,I}(z) \equiv \Omega_{\rm H\,I}(z)\rho_{\rm crit}$, q_N and q_M are related by the constraint

$$\begin{aligned}\rho_{\rm H\,I}(z) &= \int_0^\infty M_{\rm H\,I} \frac{dn_{\rm H\,I}(M_{\rm H\,I}, z)}{dM_{\rm H\,I}}\, dM_{\rm H\,I} \\ &= \int_0^\infty n_{\rm H\,I}(> M_{\rm H\,I}, z)\, dM_{\rm H\,I} \\ &= \frac{q_N(z)}{q_M(z)} \rho_{\rm H\,I}(0). \qquad (8)\end{aligned}$$

Obviously, $q_N(0) = q_M(0) = 1$.

It is not practical to explore all possible evolutionary histories for $n_{\rm H\,I}(> M_{\rm H\,I}, z)$; therefore, we restrict this work to only two scenarios.

Pure Number Density Evolution: scenario (hereafter, PNE) assumes that the H I masses of individual halos do not change at high redshift ($q_M = 1$ for all z), but only the number density of halos of a given mass changes to reflect the change in the total neutral hydrogen content of the universe, $q_N = \Omega_{\rm H\,I}(z)/\Omega_{\rm H\,I}(0)$.

Pure Mass Evolution: scenario (hereafter, PME –a direct analog of a "pure luminosity evolution" scenario in optical surveys) adopts an opposite extreme where the number density of halos remain the same ($q_N = 1$ for all z), but, instead, their masses change, $q_M = \Omega_{\rm H\,I}(0)/\Omega_{\rm H\,I}(z)$.

The justification for such a restriction is as follows. If the number density of galaxies with a given H I mass increases monotically with increasing redshift, then $q_N(z)$ is a monotonic function of z (which is expected, since galaxies merge but do not break up). If, for a given halo, its H I also increases monotically with z (which is expected, if H I gets consumed by star formation and new accretion never exceeds the consumption), then $q_M(z)$ is also a monotonic function of z. Since $q_N(0) = q_M(0) = 1$, our two scenarios bracket all possible evolutionary path for q_N and q_M.

Obviously, these assumptions do not hold all the time –for example, for some galaxies accretion of fresh gas can exceed the consumption by star formation at some times. However, over long timescales and over the whole galaxy population, it appears plausible that our two scenarios bracket the majority of evolutionary histories for $n_{\rm H\,I}(> M_{\rm H\,I}, z)$.

One more ingredient of our model can evolve with redshift –and that is the fraction of blue galaxies $f_B(M_{\rm tot})$. The measured fraction of blue galaxies at $z = 0$ from Figure 1 is exceptionally well (within the thickness of the line in Figure 1) fitted by the following simple formula:

$$f_B(M_{\rm tot}) = \left(1 + \frac{M_{\rm tot}}{M_1}\right)^{-0.25} \exp\left(-\left[\frac{M_{\rm tot}}{M_2}\right]^{0.6}\right) \qquad (9)$$

with $M_1 = 2.5 \times 10^{11}{\rm M}_\odot$ and $M_2 = 3.0 \times 10^{14}{\rm M}_\odot$. It is tempting to associate M_1 with the characteristic mass of dwarf ellipticals, and M_2 with the characteristic mass of a galaxy cluster. Then the behavior of f_B with M becomes well justified physically: for $M_{\rm tot} \gtrsim M_1$ a small fraction of all halos host dwarf and (at larger masses) regular elliptical galaxies, and f_B becomes a gradually decreasing function of mass. But for $M_{\rm tot} \gtrsim M_2$ halos turn into galaxy groups and clusters, and the fraction of halos dominated by blue galaxies plummets.

With this plausible (although by no means proven) interpretation, we can come up with reasonable evolutionary scenarios for f_B as a function of z. Specifically, we adopt the parametric form (Equation (9)), but allow M_1 and M_2 to evolve with redshift as

$$\begin{aligned}M_1(z) &= 2.5 \times 10^{11}(1+z)^\alpha {\rm M}_\odot, \\ M_2(z) &= 3.0 \times 10^{14}(1+z)^\beta {\rm M}_\odot. \qquad (10)\end{aligned}$$

It seems plausible to assume that the fraction of blue galaxies at a given halo mass is higher at high redshift, i.e., $\alpha \geq 0$ and $\beta \geq 0$. To investigate the dependence of our results on these two parameters, we consider below three representative cases with $(\alpha, \beta) = (0, 0)$, $(0, 1)$, and

$(1,1)$. This set of values is, of course, not exclusive, but it is sufficient to evaluate the robustness of our results to these parameters.

In this work we therefore consider a range of possibilities –our models A, B, and C for $\Omega_{\rm H\,I}(z)$ and two evolutionary scenarios (PNE and PME) –as sampling a plausible range of the redshift dependence of the H I mass function. It seems reasonable to speculate that the actual evolution should lie somewhere in between these different scenarios.

2.3. *Large-Scale Bias of* H I

On large scales, and not considering redshift distortions, the H I bias parameters provide the relations between the H I and dark matter correlation functions (Pan & Szapudi 2005)

$$\xi_{HI} \approx b_{1,\rm H\,I}^2 \xi_{\rm dm}, \tag{11}$$

$$\zeta_{HI} \approx b_{1,\rm H\,I}^3 \zeta_{\rm dm} + b_{2,\rm H\,I} b_{1,\rm H\,I}^2 (\xi_{\rm dm}^{(1)} \xi_{\rm dm}^{(2)} + \text{perm.}), \tag{12}$$

where ξ and ζ represent the 2-point and 3-point correlation functions, respectively. Similar relations are found for quantities calculated in Fourier space (power spectrum and bispectrum).

To calculate the large-scale bias of neutral hydrogen, we start by considering first the bias of dark matter halos with respect to the total matter clustering. In the Sheth–Tormen formalism, the bias parameters are prescriptions obtained from the spherical collapse model. For halos of mass M, the linear and (first) nonlinear terms are given by (Scoccimarro et al. 2001)

$$b_1^h(M) = 1 + \epsilon_1 + E_1, \tag{13}$$

$$b_2^h(M) = \frac{8}{21}(\epsilon_1 + E_1) + \epsilon_2 + E_2, \tag{14}$$

with coefficients given by

$$\epsilon_1 = \frac{a\nu^2 - 1}{\delta_c}, \tag{15}$$

$$\epsilon_2 = \frac{a\nu^2(a\nu^2 - 3)}{\delta_c^2}, \tag{16}$$

$$E_1 = \frac{2p}{\delta_c(1 + (a\nu^2)^p)}, \tag{17}$$

$$\frac{E_2}{E_1} = \frac{1 + 2p}{\delta_c} + 2\epsilon_1, \tag{18}$$

where $i = 1, 2$ represent the linear and first nonlinear terms, where their redshift dependence is encompassed in $\nu = \delta_c/\sigma(M, z)$, which depends on the redshift evolution of the linear power spectrum.

Using the $M_{\rm H\,I} - M_{\rm tot}$ relation obtained in the previous section, the H I bias from all halos with a mass greater than $M_{\rm min}$ is given by the following integral:

$$b_{i,\rm H\,I} = \frac{1}{\rho_{\rm H\,I}} \int_{M_{\rm min}}^{\infty} dM n_h(M) b_i^h(M) \langle M_{\rm H\,I}(M) \rangle . \tag{19}$$

where $\rho_{\rm H\,I}$ is the density of neutral hydrogen:

$$\rho_{\rm H\,I} = \int_{M_{\rm min}}^{\infty} dM n_h(M) \langle M_{\rm H\,I}(M) \rangle . \tag{20}$$

In what follows we present the analytic results for the large-scale bias and its evolution in redshift.

3. RESULTS

3.1. *Analytic Results*

We calculate the bias parameters as a function of redshift for all models described in §2.2. In Figure 4 we show the results for the models where the galaxy blue fraction does not evolve with redshift, i.e., in Equation (10), $\alpha = \beta = 0$. In the left panel we present the linear (b_1) bias redshift evolution; in the right panel, the nonlinear (b_2) bias evolution, with $M_{\rm min} = 10^4\ h^{-1}{\rm M}_\odot$, which, given the fact that it is not expected that low mass halos (below $10^7\ h^{-1}{\rm M}_\odot$) contain significant amounts of H I, is set to the value mentioned above as a conservative limit. The black thick line shows the evolution of bias in the PME scenario; as for the PNE scenario, the red thin solid line shows the results for model A, the magenta dashed line shows results for model B, and the blue dotted line does it for model C.

The first feature that arises from these analytical results is the strong dependence of the bias terms on the redshift for all the models considered. Given that $\Omega_{\rm H\,I}$ does not evolve significantly with redshift, the reason for this behavior lies in the fact that preserving the matching relations (Equation (4)) at higher redshift has the consequence that the most massive halos, which are less numerous at high redshift (i.e., are more biased with respect to the dark matter distribution), carry more H I mass than the halos with the same $M_{\rm tot}$ at $z = 0$. Therefore, it is expected for both b_1 and b_2 to show a strong redshift dependence.

For the PNE scenario, we can see differences in both bias parameters, though they are relatively small. Between models A and B, the differences are increasing with redshift, with a peak around $z \sim 2$ –at the moment where $\Omega_{\rm H\,I}(z)$ of model B is the lowest compared to the rest of the models; since the fraction of neutral hydrogen in that model is low, in the PNE scenario this implies fewer halos, and therefore the bias is expected to be larger. In model C, the difference in the bias evolution compared to model A appears only at low redshifts, since it starts with a higher $\Omega_{\rm H\,I}$ and therefore having a smaller bias on redshifts close to $z = 0$. The differences for the nonlinear bias term b_2 are qualitatively similar but much milder.

As opposed to the PNE scenario, there are no differences between the models biases in the PME scenario; this is not surprising since, by definition, in that scenario just the masses of halos change, but not their total number density. Hence, irrespective of the $\Omega_{\rm H\,I}(z)$ evolution, the behavior of the bias here depends only on the cosmological evolution. When we compare both scenarios, the differences in the bias parameter b_1, albeit small in general, grow steadily with redshift reaching 10% level between $z = 1$ and 4; note here that there are differences between the PME scenario and the model B in the PNE scenario only after $z \sim 2$. For b_2 between $z = 0$ and 1 there are almost no differences between the models, but after that the differences grow until reaching almost a factor of 2 by $z = 4$. In both cases the PME scenario has a larger bias; this difference is due to the fact that more halos are needed in the PNE scenario to account for the change of neutral hydrogen in the universe, which leads to a lower halo mass for a given H I mass and hence a smaller bias than in the PME scenario.

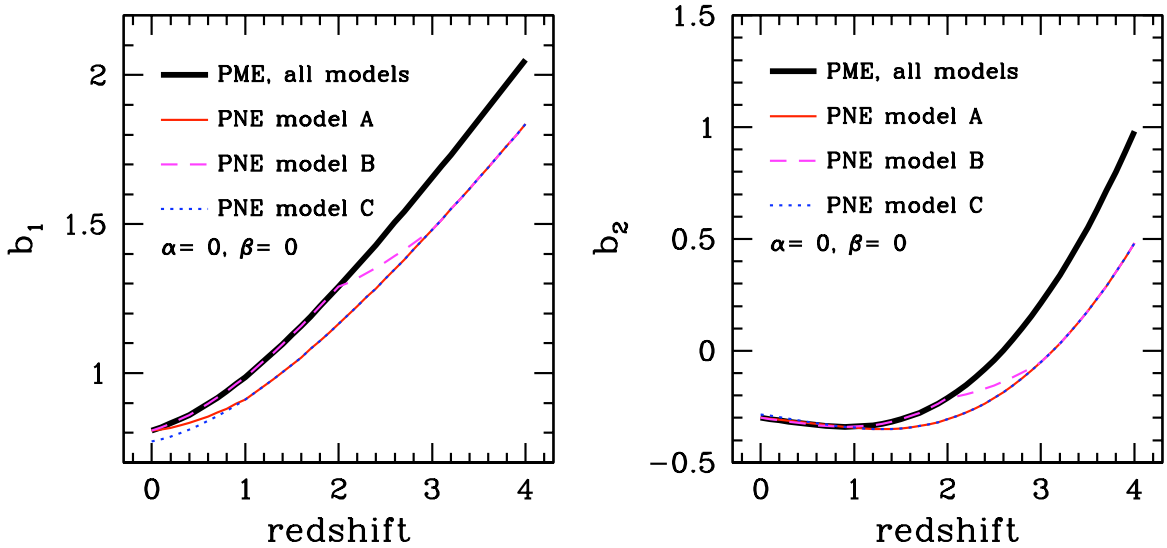

FIG. 4.— Bias coefficients of neutral hydrogen clouds as a function of redshift. *Left:* linear bias b_1 vs. redshift in the pure mass evolution scenario for all models (thick black solid line), and the pure number evolution scenario for model A (thin red solid line), model B (dashed magenta line) and model C (blue dotted line). *Right:* first nonlinear bias term b_2 vs. redshift for the same models described in the left plot. All coefficients are calculated with $M_{\rm min} = 10^4\ h^{-1}{\rm M}_\odot$.

As for the differences between the different blue fraction evolution models, and the case where we simply assume all galaxies contain H I, we show in Figure 3.1 the quantity

$$\Delta b_i = b_i - b_{i,{\rm FID}}, \tag{21}$$

where $i = 1, 2$, and the fiducial (FID) model corresponds to the model A in the PNE scenario, with $(\alpha, \beta) = (0, 0)$. The black dotted line represents the $f_B(M, z) = 1$, i.e. all galaxies carry H I; the blue short-dashed line represents the evolution model with $(\alpha, \beta) = (0, 1)$, and the long-dashed line shows the results for the blue fraction evolution model with $(\alpha, \beta) = (1, 1)$, both in the model A of the PNE scenario. For other models and scenarios the results are qualitatively similar: between the different blue fraction evolution models both the linear and nonlinear bias do not differ significantly. But when we compare our FID model to that where all galaxies carry neutral hydrogen, i.e., $f_B = 1$, then the differences are more significant, considering a realistic blue galaxy fraction lowers the H I bias, since the neutral hydrogen avoids accumulating in the bigger halos and concentrates more in mid-size and small mass halos.

The weak dependence of the H I bias on the model adopted for the neutral hydrogen evolution means that the intensity mapping observations will be able to provide only a limited amount of information on the global evolution of the neutral hydrogen abundance in the universe. On the other hand, from a cosmologist's point of view, this is good news: a detailed knowledge of the H I evolution may not be needed for studying the dark energy evolution in the radio intensity mapping experiments. Note that even though the differences in b_2 between the PME and PNE models at high redshift are larger than those in b_1, measurements on higher-order correlations have larger uncertainties which would make the b_2 estimations less reliable. Nevertheless, if good signal-to-noise measurements can be done, this parameter can play a relevant role in determining the right evolution model.

3.2. *Linear Bias calculated from simulations*

In order to have a consistency check of our analytical calculations, we turn to estimate the linear H I bias from the Millennium Simulation (Springel et al. 2005). The N-body simulation was carried out for 2160^3 particles with mass $m_p = 8.6 \times 10^8\ h^{-1}{\rm M}_\odot$ in a box with $L_{\rm box} = 500\ h^{-1}$Mpc on the side, with the same cosmological parameters we use for our analytical estimates.

Following Equation (11), we can estimate the linear bias in the simulation by

$$b^{\rm MS}_{{\rm H\,I},1}(k) = \sqrt{\frac{P_{\rm H\,I}(k)}{P_{\rm dm}(k)}}, \tag{22}$$

where $P_{\rm dm}(k)$ is the real-space dark matter power spectrum and $P_{\rm H\,I}(k)$ is the real-space HI power spectrum. In addition to validate our analytical method, this measurement should allow us to estimate the scales below which nonlinear effects become relevant.

We use the $M_{\rm H\,I} - M_{\rm tot}$ relation obtained in §2.2 to assign the neutral hydrogen mass to dark matter halos and calculate the H I power spectrum $P_{\rm H\,I}$. Note that due to the mass resolution of the simulation, our dark matter halo catalog does not resolve well the halos below a certain mass threshold, and those halos may contribute substantially to the value of the H I bias. Therefore, consistency requires the bias measured in the Millennium Simulation to be compared to the value obtained analytically through Equation (19) assuming the *same* mass threshold $M_{\rm min}$. For this reason, we compare analytical estimates and measured values of the bias obtained by assuming $M_{\rm min} \sim 10^{11} h^{-1} M_\odot$, which should correspond to halos with $N_p \sim 100$ particles. Another aspect when we are "painting" H I in the simulation is its distribution inside the halos. In our case, we place all hydrogen at the center of the halo, i.e we are not assuming diffuse H I emission inside. While this might not model accurately the small-scale clustering of the H I, what matters in the large-scale clustering are the details of the $M_{\rm H\,I} - M_{\rm tot}$ re-

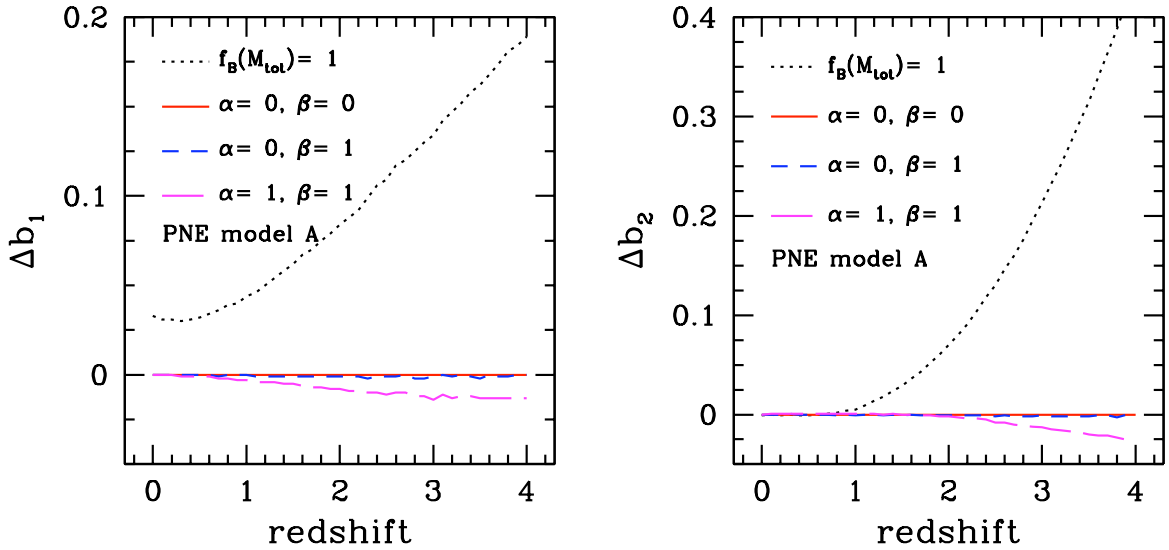

FIG. 5.— Differences in the bias parameters (linear b_1 in left panel, nonlinear $b_2$in right panel) between different blue fraction redshift evolution models. The FID model is the model A in the PNE scenario, with $(\alpha, \beta) = (0, 0)$, in red straight line. *Left:* $\Delta b_1 = b_1 - b_{1,\rm FID}$, where the black dotted line represents the $f_B(M, z) = 1$, the blue short-dashed line represents the evolution model with $(\alpha, \beta) = (0, 1)$, and the long-dashed line shows the results for the blue fraction evolution model with $(\alpha, \beta) = (1, 1)$. *Right:* $\Delta b_2 = b_2 - b_{2,\rm FID}$, lines represent the same models of the left panel.

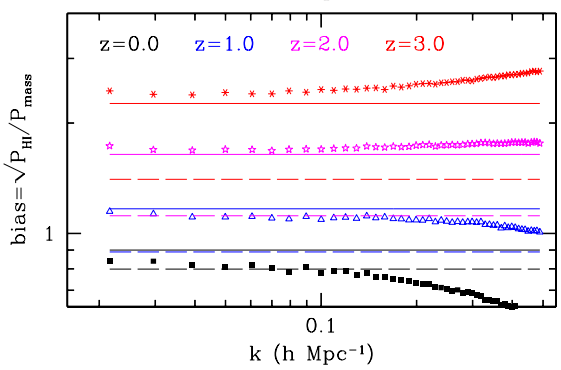

FIG. 6.— Neutral hydrogen bias factor $b^{\rm MS}_{\rm H\,I,1}(k)$ at different redshifts from the Millennium Simulation (symbols) for the model A in the PNE scenario, and our analytical predictions for the linear bias $b_{1,\rm H\,I}$ (horizontal lines). The dashed lines show analytical predictions for the whole set of halos ($M_{\rm min} = 10^4\ h^{-1}{\rm M}_\odot$), while solid lines show the analytical calculations for the set of halos resolved in the Millennium Simulation ($M_{\rm min} = 10^{11} h^{-1} M_\odot$).

lation; the spatial profile of the neutral hydrogen within a halo will have a very limited effect on the measured bias and its scale dependence on large scales we present in this paper (Cooray & Sheth 2002; Schulz & White 2006).

Figure 6 shows, in symbols, the measured bias $b^{\rm MS}_{\rm H\,I,1}(k)$ for a series of redshifts from $z = 0$ to $z = 3$ for the model A in the PNE scenario. The solid lines represent $b_{\rm H\,I,1}$ from our analytical modeling, with a minimum mass cut $M_{\rm min} = 10^{11}\ h^{-1}{\rm M}_\odot$; the dashed lines are the results of $b_{\rm H\,I,1}$ with $M_{\rm min}$=$10^4\ h^{-1}{\rm M}_\odot$.

The bias measured from the simulation using Equation (22) should agree with $b_{\rm H\,I,1}$ obtained from Equation (19) on large scales; on smaller scales, a contribution from the clustering within a halo results in a scale dependence in bias (Seljak 2000) which we refer to as a nonlinear bias effect. From the figure, we indeed observe a strong redshift evolution of large-scale bias in agreement with the behavior found in our analytical calculations; the agreement is of the order of 5%. The small differences are due mainly to the fact that our analytical halo mass function, though is a good approximation, indeed has small differences to the one measured in simulations. The figure also shows that the linear bias assumptions break down for $k \gtrsim 0.15\,h{\rm Mpc}^{-1}$, but the effective nonlinear scale (where the linear bias deviates strongly from a constant value) appears to evolve little with redshift, likely a consequence of our adopted $M_{\rm H\,I} - M_{tot}$ relationship, given the fact that in simulations this scale varies greatly with redshift. We point out that if our assumption of the one-to-one correspondence between the HIPASS source and the halo breaks down for large halo masses, it will alter $b^{\rm MS}_{\rm H\,I,1}(k)$ to some extent.

As stated earlier, the difference between the two sets of horizontal lines in Figure 6 shows the contribution of halos with $M_{\rm tot} < M_{\rm min} = 10^{11} h^{-1} M_\odot$. This contribution is substantial. It is important to note that in the case of the 21 cm intensity mapping, we suffer no lower detection limit in neutral hydrogen mass and therefore halo mass. In that case, the bias derived with $M_{\rm min} = 0$ is the appropriate one. As a much higher mass resolution would be required to reduce $M_{\rm min}$ much below $10^{11} h^{-1} M_\odot$, the Millennium Simulation –or another simulation with similar resolution– cannot be used to provide an accurate estimate for the H I bias for this kind of survey, but only as a useful tool to validate the semi-analytical estimates obtained in the previous section.

3.3. *Impact of bias evolution on the power spectrum*

Having shown how the H I bias evolves with redshift, we turn to assess to what extent this may or may not have an effect on the measurement of the power spectrum. At tree-level in perturbation theory, the density fluctuations in the neutral hydrogen $\delta_{\rm H\,I}$ and in the dark matter $\delta_{dm} \equiv \delta$ are related through

$$\begin{aligned}\delta_{\rm H\,I}(\vec{x}, \chi) &= b(\chi)\delta(\vec{x}, \chi) = b(\chi) D_+(\chi)\delta(\vec{x}, 0) \\ &\equiv E(\chi)\delta(\vec{x}, 0),\end{aligned} \tag{23}$$

where $D_+(\chi)$ is the linear growth factor, and we exchanged redshift z for comoving distance χ. When observations are performed, only the product $E(\chi)$ can be measured, as the redshift evolution of the bias contributes a component that combines with the growth of structure. To understand to what extent this has an influence on the measurement of the power spectrum, we start by Taylor expanding $E(\chi) = \sum E_0^{(n)} \chi^n / n!$, where all derivatives $E_0^{(n)} = d^n E / d\chi^n$ are evaluated at the observer's position. Next, we Fourier transform $\delta_{\rm H\,I}(\vec{x})$ to obtain

$$\begin{aligned}\delta_{\rm H\,I}(\vec{k},\chi) &= \int d^3\vec{x}\, e^{-i\vec{k}\cdot\vec{x}} \delta_{\rm H\,I}(\vec{x},\chi) \\ &= \int d^3\vec{x}\, e^{-i\vec{k}\cdot\vec{x}} \left[\sum_{n=0}^{\infty} \frac{E_0^{(n)}\chi^n}{n!}\right] \delta(\vec{x},0) \\ &= \sum_{n=0}^{\infty} \frac{i^n E_0^{(n)}}{n!} \partial_{k_\parallel}^n \delta(\vec{k},0), \end{aligned} \tag{24}$$

where we used the fact that $\chi^n = i^n \partial_{k_\parallel}^n e^{-i\vec{k}\cdot\vec{x}}$. Next we note that $\delta(\vec{k},0)$ is a Gaussian random variable with dispersion $\sigma_{\delta(\vec{k},0)} = \sqrt{P(k,0)}$. We can then rewrite it as $\delta(\vec{k},0) = \sqrt{P(k,0)}\lambda_{\vec{k}}$ with $\lambda_{\vec{k}}$ a Gaussian random variable with $\langle\lambda_{\vec{k}}\rangle = 0$ and $\langle\lambda_{\vec{k}}\lambda^*_{\vec{k}'}\rangle = (2\pi)^3\delta_D^3(\vec{k}-\vec{k}')$. Note that $\vec{k}$ for $\lambda_{\vec{k}}$ is nothing but a label and that all the dependence of $\delta(\vec{k},0)$ on the wavevector is really encoded in the prefactor. Defining the H I power spectrum by $\langle\delta_{\rm H\,I}(\vec{k},\chi)\delta^*_{\rm H\,I}(\vec{k}',\chi)\rangle \equiv P_{\rm H\,I}(k,\chi)\,(2\pi)^3\,\delta_D^3(\vec{k}-\vec{k}')$ we can then express $P_{\rm H\,I}$ as

$$P_{\rm H\,I}(k,\chi) \approx \left[L(k) + \mu^2 H(k)\right] P(k,0), \tag{25}$$

where $\mu = \cos(\theta)$ is the cosine of the angle the wavevector $\vec{k}$ makes with the line of sight and $L(k)$ and $H(k)$ are the first two terms that encode the χ dependence of $\delta_{\rm H\,I}$. We calculate the first few terms of L and H using the fact that $k_\parallel = k\cos(\theta) = k\mu$ and $\vec{k}_\perp = k\sin(\theta) = k\sqrt{1-\mu^2}$. They turn out to be

$$L \approx E_0^2 - E_0 E_0'' \frac{P'}{2kP}, \tag{26}$$

$$H \approx E_0 E_0'' \left(\frac{P'^2}{4P^2} - \frac{P''}{2P} + \frac{P'}{2kP}\right) + E_0'^2 \frac{P'^2}{4P^2}, \tag{27}$$

where P' and P'' denote first and second derivatives of P with respect to k, while E_0' and E_0'' denote derivatives of $E(\chi)$ with respect to the comoving distance evaluated at the observer position. In general, the comoving distance dependence generates in the power spectrum a directionality dependence that is reminiscent of redshift space distortions. Despite that the nature of the effect considered here is completely different from the one of redshift space distortions (which is due to peculiar velocities), the two effects may be in practice difficult to separate from one another, unless we have a sufficiently small sample variance on the clustering measurement. However, we point out that the n-th derivative with respect to the comoving distance scales as H_0^n and therefore $E_0' \sim 10^{-4}$ and $E_0'' \sim 10^{-8}$. As such, all but the first term appearing in Equations (26) and (27) are of order 10^{-8} and only the E_0^2 term appearing in L will give a non-negligible contribution. Also, it is possible to note that the above treatment is valid even in the case of a perfect unbiased dark matter tracer.

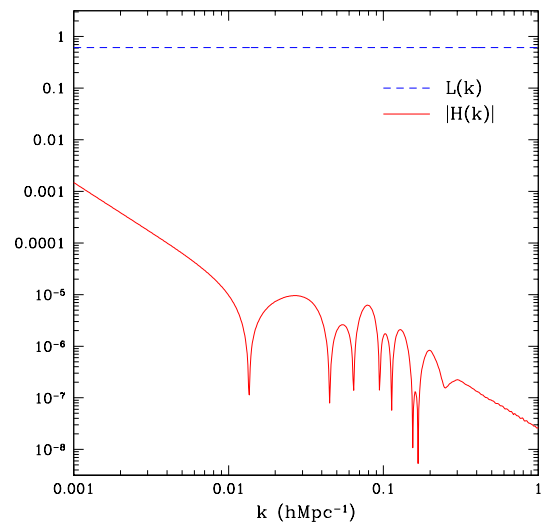

FIG. 7.— First two correction coefficients $L(k)$ and $|H(k)|$.

In Figure 7 we show the functions $L(k)$ and $|H(k)|$. Consistent with the above estimates, H turns out to be extremely small. On the other hand, L is dominated by the term E_0^2 and therefore does not show any appreciable k dependence, except for extremely large scales $k \sim 10^{-3}$, where it deviates from E_0^2 by about 0.3%. These two facts together allow us to conclude that the measurement of the 21 cm power spectrum through intensity mapping should not be sensibly affected by the redshift dependence of the bias.

4. SUMMARY AND CONCLUSIONS

In this paper we have estimated analytically and in the Millennium Simulation the large-scale bias of neutral hydrogen from a non-parametric model which establish a one-to-one relation between the total mass and the H I mass of galactic halos. Although only an approximation, this relation is expected to hold for a large range of masses.

The bias parameters have been calculated using a model which uses elements of the HOD formalism, in a way that can be considered complementary to the galaxy-HOD model of H I galaxies carried out by Wyithe et al. (2009); we do not deal in our case with the individual galaxies inside dark matter halos but with the total neutral hydrogen inside them. In terms of large-scale clustering, these approaches are completely equivalent.

Using this approach together with different models for the redshift evolution of the H I content in the universe and the relation between neutral hydrogen and total matter contents of galactic halos, we analyze the evolution of bias with redshift. We find that both linear and non-linear bias increase significantly with redshift. This contrasts with the finding by Wyithe et al. (2008b), based on an extrapolation to lower redshifts from a reionization model of Wyithe & Loeb (2008). Since Wyithe et al. (2008b) do not account for clustering of galactic halos

that host all neutral hydrogen after reionization, they underestimate the H I bias at $z \lesssim 4$. On the other hand, our results are in agreement with the high value of the linear large-scale bias at redshift $z \sim 3$ measured in the model by Bagla & Khandai (2009) where they populate H I in high-resolution $N-$body simulations.

We also find that, given the limitations of our model at high masses, the estimation of the bias does not change significantly when the very high mass halos are neglected.

Our main conclusion is that, despite a wide range of possible models for the evolution of H I mass function that we consider, in all models the bias evolution is similar –the neutral hydrogen distribution is mildly antibiased at $z = 0$ but becomes strongly biased ($b_{\rm H\,I} \sim 2$) by $z \sim 4$. This result is encouraging for the planned radio intensity mapping experiments, since large bias implies a stronger 21 cm signal. Nevertheless, this strong redshift evolution does not significantly compromise the measurements of the neutral hydrogen power spectrum along the radial direction.

We thank Gerard Lemson for his support and patience in providing the Millennium Simulation halo catalogs. We also thank Andrey Kravtsov for his comments and suggestions.

This work was supported in part by the Kavli Institute for Cosmological Physics at the University of Chicago through grants NSF PHY-0114422 and NSF PHY-0551142 and an endowment from the Kavli Foundation and its founder Fred Kavli. AV and HS are supported by the DOE at Fermilab. The Millennium Simulation databases used in this paper and the web application providing online access to them were constructed as part of the activities of the German Astrophysical Virtual Observatory.

REFERENCES

Ansari, R., Le Goff, J., Magneville, C., Moniez, M., Palanque-Delabrouille, N., Rich, J., Ruhlmann-Kleider, V., & Yèche, C. 2008, arXiv:0807.3614
Bagla, J. S., & Khandai, N. 2009, ArXiv e-prints
Barkana, R., & Loeb, A. 2007, Reports on Progress in Physics, 70, 627
Berlind, A. A., & Weinberg, D. H. 2002, ApJ, 575, 587
Bildfell, C., Hoekstra, H., Babul, A., & Mahdavi, A. 2008, MNRAS, 389, 1637
Blake, C., & Glazebrook, K. 2003, ApJ, 594, 665
Chang, T., Pen, U., Peterson, J. B., & McDonald, P. 2008a, Physical Review Letters, 100, 091303
Chang, T.-C., Pen, U.-L., Peterson, J. B., & McDonald, P. 2008b, Physical Review Letters, 100, 091303
Colín, P., Klypin, A. A., Kravtsov, A. V., & Khokhlov, A. M. 1999, ApJ, 523, 32
Conroy, C., & Wechsler, R. H. 2009, ApJ, 696, 620
Conroy, C., Wechsler, R. H., & Kravtsov, A. V. 2006, ApJ, 647, 201
Cooray, A., & Sheth, R. 2002, Phys. Rep., 372, 1
Eisenstein, D. 2002, in Astronomical Society of the Pacific Conference Series, Vol. 280, Next Generation Wide-Field Multi-Object Spectroscopy, ed. M. J. I. Brown & A. Dey, 35–+
Eisenstein, D. J., Hu, W., & Tegmark, M. 1998, ApJ, 504, L57+
Furlanetto, S. R., Oh, S. P., & Briggs, F. H. 2006, Phys. Rep., 433, 181
Gnedin, N. Y. 2008, ApJ, 673, L1
Guo, Q., White, S., Li, C., & Boylan-Kolchin, M. 2009, ArXiv:0909.4305
Hu, W., & Haiman, Z. 2003, Phys. Rev. D, 68, 063004
Hu, W., & White, M. 1996, ApJ, 471, 30
Kravtsov, A. V., Berlind, A. A., Wechsler, R. H., Klypin, A. A., Gottlöber, S., Allgood, B., & Primack, J. R. 2004, ApJ, 609, 35
Kravtsov, A. V., & Klypin, A. A. 1999, ApJ, 520, 437
Linder, E. V. 2003, Phys. Rev. D, 68, 083504
Loeb, A., & Wyithe, S. 2008, Phys. Rev. Lett., 100, 161301
Mao, Y., Tegmark, M., McQuinn, M., Zaldarriaga, M., & Zahn, O. 2008, Phys. Rev. D, 78, 023529
Marín, F. A., Wechsler, R. H., Frieman, J. A., & Nichol, R. C. 2008, ApJ, 672, 849
Metha et al. 2010, in preparation
Montero-Dorta, A. D., & Prada, F. 2009, MNRAS, 399, 1106
Nagai, D., & Kravtsov, A. V. 2005, ApJ, 618, 557
Obreschkow, D., Croton, D., D eLucia, G., Khochfar, S., & Rawlings, S. 2009, ApJ, 698, 1467
Padmanabhan, N., & White, M. 2009, Phys. Rev. D, 80, 063508
Pan, J., & Szapudi, I. 2005, MNRAS, 362, 1363
Pritchard, J. R., & Loeb, A. 2008, Phys. Rev. D, 78, 103511
Prochaska, J. X., Herbert-Fort, S., & Wolfe, A. M. 2005, ApJ, 635, 123
Prochaska, J. X., & Wolfe, A. M. 2009, ApJ, 696, 1543
Rao, S. M., Turnshek, D. A., & Nestor, D. B. 2006, ApJ, 636, 610
Schulz, A. E., & White, M. 2006, Astroparticle Physics, 25, 172
Scoccimarro, R., Sheth, R. K., Hui, L., & Jain, B. 2001, ApJ, 546, 20
Seljak, U. 2000, MNRAS, 318, 203
Seo, H., Dodelson, S., Marriner, J., Mcginnis, D., Stebbins, A., Stoughton, C., & Vallinotto, A. 2010, submitted to ApJ, arXiv:0910.5007
Seo, H., & Eisenstein, D. J. 2003, ApJ, 598, 720
Sheth, R. K., Mo, H. J., & Tormen, G. 2001, MNRAS, 323, 1
Sheth, R. K., & Tormen, G. 2002, MNRAS, 329, 61
Springel, V. et al. 2005, Nature, 435, 629
Tinker, J. L., & Conroy, C. 2009, ApJ, 691, 633
Visbal, E., Loeb, A., & Wyithe, S. 2008, arXiv:0812.0419
Volonteri, M., & Gnedin, N. 2009, ArXiv:0905.0144
Wyithe, J. S. B., & Loeb, A. 2008, MNRAS, 383, 606
Wyithe, J. S. B., Loeb, A., & Geil, P. M. 2008a, MNRAS, 383, 1195
—. 2008b, MNRAS, 383, 1195
Wyithe, S., Brown, M. J. I., Zwaan, M. A., & Meyer, M. J. 2009, arXiv:0908.2854
Zwaan, M. A., Meyer, M. J., Staveley-Smith, L., & Webster, R. L. 2005, MNRAS, 359, L30

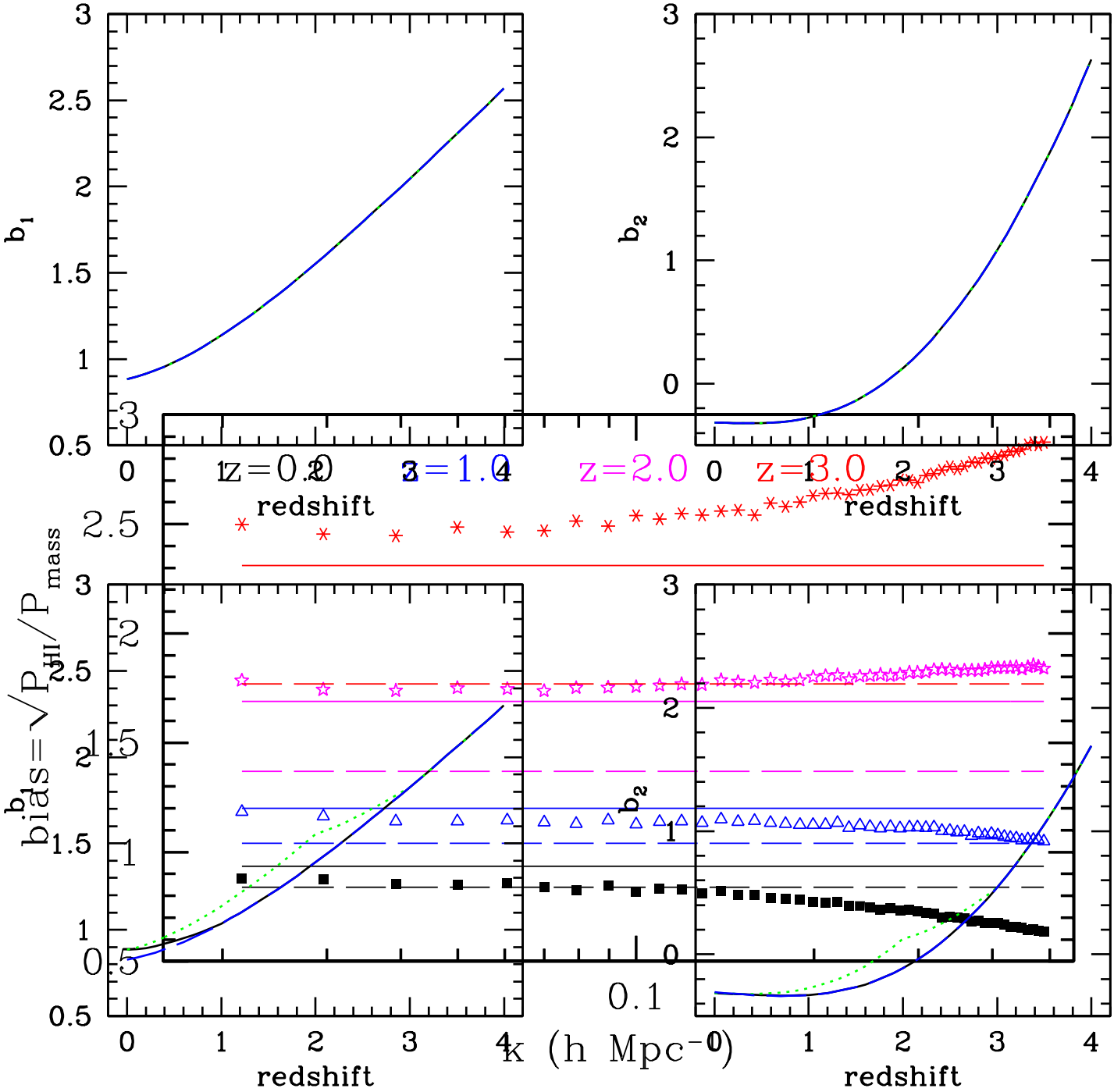
b1
b2
redshift
z=0.0
z=1.0
z=2.0
z=3.0
bias=√P_HI/P_mass
k (h Mpc⁻¹)

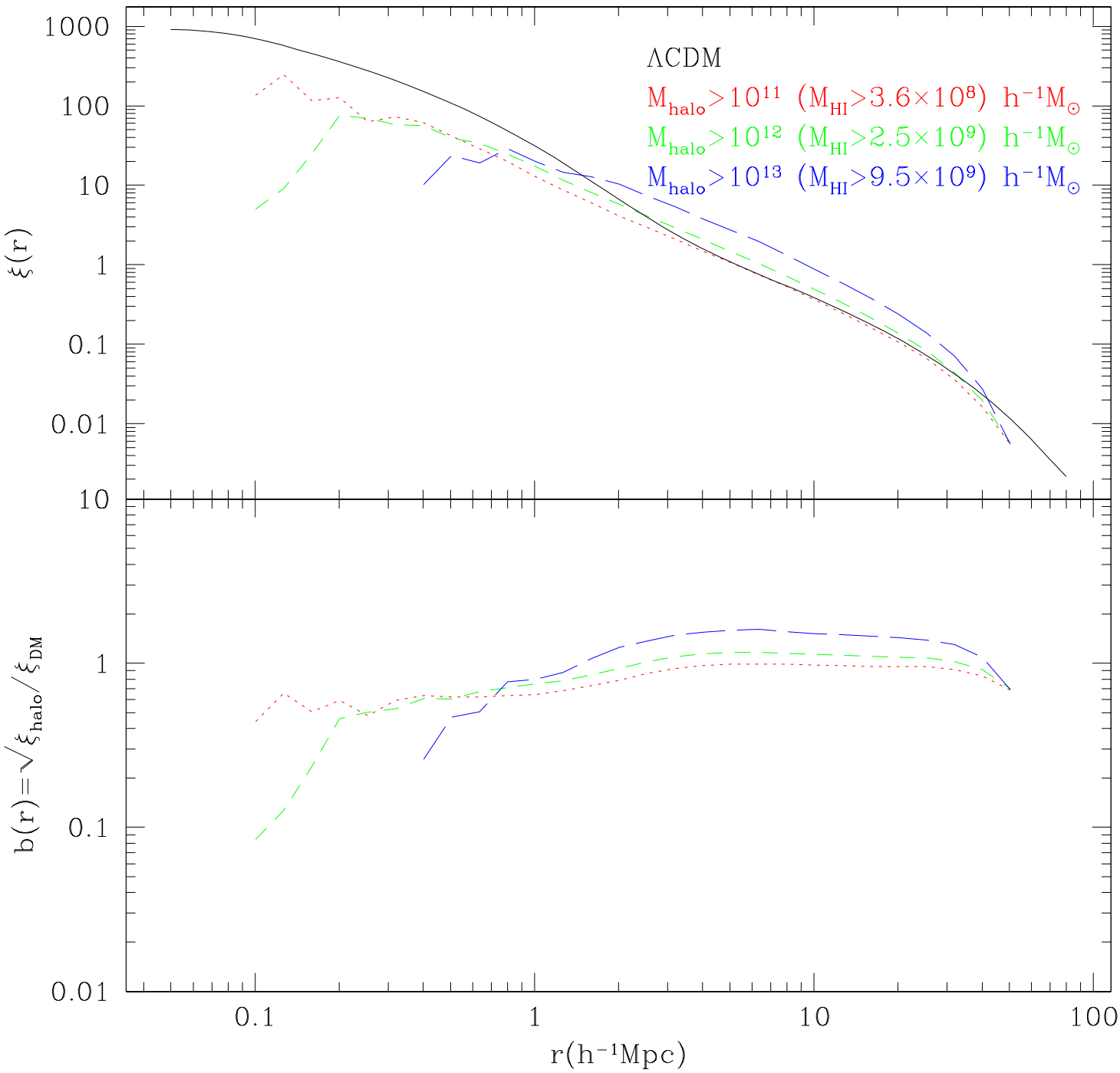
ΛCDM
M_halo>10^11 (M_HI>3.6×10^8) h^-1M_⊙
M_halo>10^12 (M_HI>2.5×10^9) h^-1M_⊙
M_halo>10^13 (M_HI>9.5×10^9) h^-1M_⊙
ξ(r)
b(r)=√ξ_halo/ξ_DM
r(h^-1Mpc)
1000
100
10
1
0.1
0.01
0.1
1
10
100

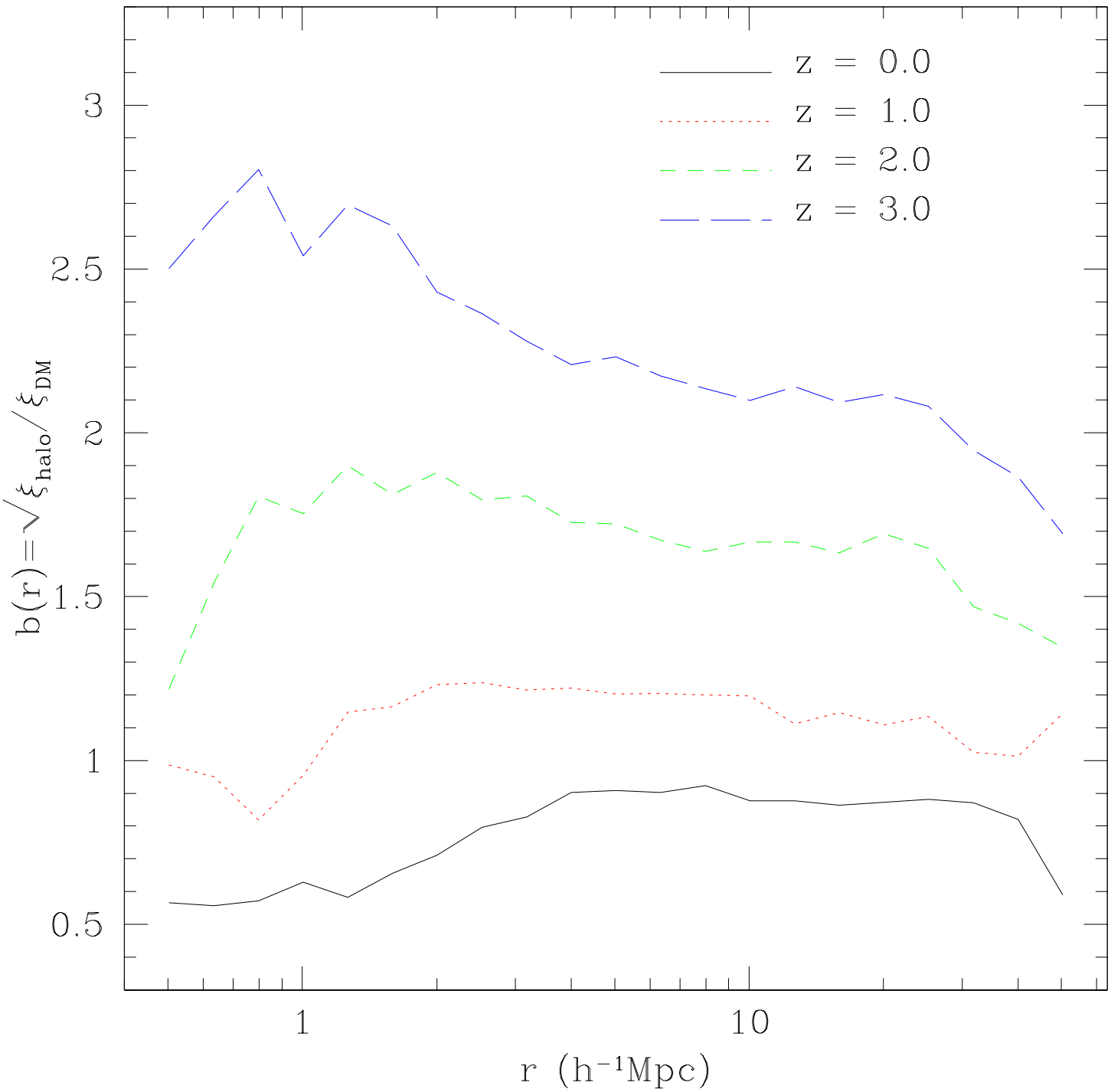
z = 0.0
z = 1.0
z = 2.0
z = 3.0
3
2.5
2
1.5
1
0.5
1
10
$b(r) = \sqrt{\xi_{halo}/\xi_{DM}}$
r (h^{-1}Mpc)

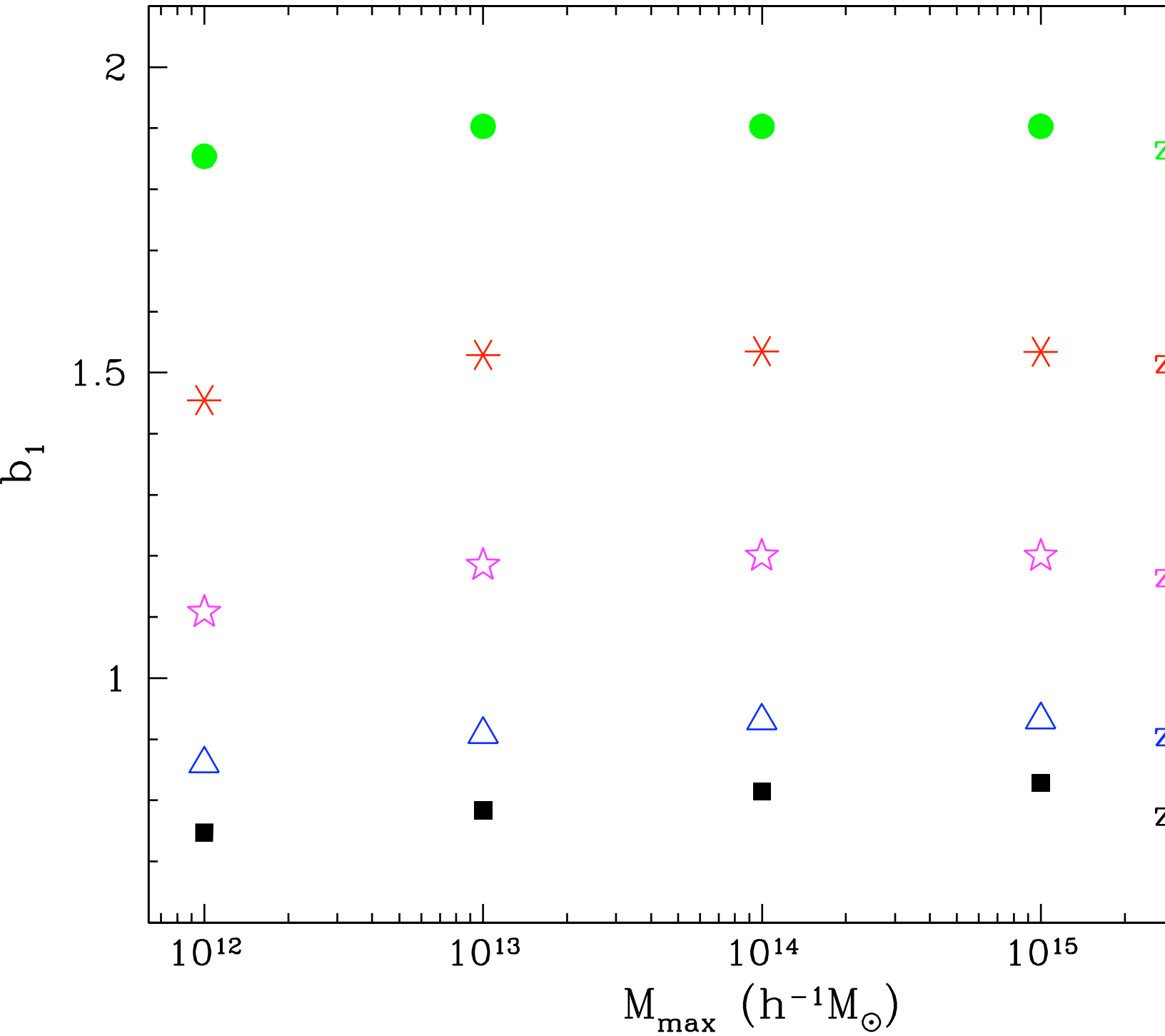
2
1.5
1
b_1
10^{12}
10^{13}
10^{14}
10^{15}
M_{max} $(h^{-1}M_\odot)$
z
z
z
z